redin Revista Facultad de Ingeniería, Universidad de Antioquia, No. 84, pp. 27-34, 2017

Biocompatibility of bismuth silicate coatings deposited on 316L stainless steel by sol-gel process

Biocompatibilidad de recubrimientos de silicato de bismuto depositados sobre sustratos de acero inoxidable 316L por sol-gel

Jorge Hernando Bautista-Ruiz[1, 2*], Jhon Jairo Olaya-Flórez[1], Willian Arnulfo Aperador-Chaparro[3]

[1] Facultad de Ingeniería, Universidad Nacional de Colombia. Carrera 45 # 26-85. C. P. 111321. Bogotá, Colombia.
[2] Departamento de Física, Facultad de Ciencias Básicas, Universidad Francisco de Paula Santander. Av. Gran Colombia # 12E-96. C. P. 540003. Cúcuta, Colombia.
[3] Facultad de Ingeniería, Universidad Militar Nueva Granada. Carrera 11 # 101-80. C. P. 110211. Bogotá, Colombia.

ARTICLE INFO
Received Februrary 07, 2017
Accepted August 02, 2017

KEYWORDS
MTT assay, bismuth silicate films, sol-gel, biocompatibility

Ensayo MTT, películas de silicato de bismuto, sol-gel, biocompatibilidad

ABSTRACT: Bismuth silicate, (BSO) thin films have been fabricated by sol–gel process. The stable sol was synthesized by using bismuth nitrate (III) pentahydrate and tetraethyl orthosilicate (TEOS). The films were deposited by spin-coating at 1500 rpm on Stainless Steel 316L. The films were characterized by Atomic Force Microscopy (AFM), Scanning Electron Microscopy (SEM), X-ray diffraction (XRD) besides the measured of the films thickness. This study aimed to evaluate the cell adhesion and cellular proliferation of osteoblast cells on BSO thin films and substrate 316L by MTT assay. It is concluded that the growth of osteoblasts is homogeneous in the surface of the coatings indicating that the medium offered by the films does not present active cytotoxicity and exceed in large number the level of cellular growth compared to Stainless Steel.

RESUMEN: Películas delgadas de silicato de bismuto (BSO) se han fabricado mediante el proceso sol-gel. El sol estable se sintetizó utilizando nitrato de bismuto (III) pentahidrato y tetraetil-ortosilicato (TEOS). Las películas fueron depositadas a 1500 rpm mediante la técnica de centrifugado. Los recubrimientos se caracterizaron por microscopía de fuerza atómica (AFM), microscopía electrónica de barrido (SEM), difracción de rayos-X (DRX) y se midió el espesor de las películas. El objetivo de este estudio fue evaluar la adhesión y la proliferación en células de osteoblastos, mediante el ensayo MMT, al incubarse sobre películas BSO en sustratos de 316L. Se concluyó que el crecimiento de los osteoblastos es homogéneo en la superficie de las películas, indicando que el medio ofrecido por los recubrimientos no presenta actividad citotóxica y favorece los niveles de crecimiento celular en comparación con los resultados obtenidos para los sustratos de acero inoxidable.

1. Introduction

Bismuth oxide (Bi_2O_3) has several α-monoclinic, ß-tetragonal, γ-centred (bcc) and δ-centred cubic crystalline structures (fcc). The stability of each phase depends on different conditions such as temperature, heat treatment and chemical doping [1, 2]. Among the phases of bismuth oxide, the γ-bcc phase is of great interest because of its purity and metastability. This compound is formed during the cooling of the fcc δ phase of high stability at high temperatures [2]. In order to stabilize the γ phase, a small amount of other cations is added to form a new compound of type $Bi_{12}MO_{20}$ (BSO) belonging to the sillenite family, where M represents the doping cations (M = Si, Ge, Ti, Pb, Mn, $B_{1/2}$) [2-5]. The BSO crystallizes in the cubic phase, spatial group I23, which is not midway-symmetric [6]. The particularity of this phase is that the tetrahedral silicon-oxygen is located in the core and in the corners of the unit cell. The entire structure of the BSO crystal is composed of 7-oxygen coordinated with Bi polyhedral and SiO_4 tetrahedral [6].

The sol-gel method is a process of material synthesis that arouses great interest in the field of research [7]. The sol-gel concept is related to the process by which solid particles are dispersed in a liquid medium (sol, at the highest colloidal percentage) agglomerated to form a continuous three-dimensional (3D) network bounded by the container containing the liquid (Gel) [8]. The process

* Corresponding author: Jorge Hernando Bautista Ruiz
e-mail: jorgebautista@ufps.edu.co
ISSN 0120-6230
e-ISSN 2422-2844
DOI: 10.17533/udea.redin.n84a04

of sol to gel consists of three fundamental steps: the preparation of the sun, the gelation of the same, and the elimination of the solvents [7]. The sols can be synthesized from inorganic salts or molecular precursors called metal alkoxides. In the system, a molecular network grows due to mainly hydrolyzed condensation reactions, and the microstructure formed from the experimental conditions. To control the reaction and hydrolysis rates, water is added to the molecular precursor in the presence of an acid or basic catalyst [7]. The sol-gel method has been widely applied in the production of various materials ranging from purely inorganic materials to organic and biological systems, that allow the development of biosensors used in medical diagnosis [9, 10], superhydrophobic and superficial superphobic studies [11], superconductors [12, 13], fuel cells [14, 15], ceramic compounds [16], dental ceramics [17] and other materials, in a wide range of compositions. Sol-gel technology has found great potential for applications in the scientific and technological fields because the processes can be developed at room temperature, the combination of properties and the enormous advantages inherent in greater homogeneity and purity, easier control in size and form of the final material, and greater manageability [9, 18].

The application of steels such as the AISI 316L widely used in surgical implantology, for its low cost compared to other materials such as titanium. Due to the corrosive susceptibility in contact with solutions containing chlorine ions, it is considered as a public health problem. Steel when implanted in the human body is subjected to corrosive environments caused by the conditions of the physiological fluids in contact. When it undergoes corrosive attack, the iron diffuses in the body. Excess iron in the body can cause hemosiderosis (an increase of iron in the tissue without alteration of its structure or function), or hemochromatosis (in which the tissue is damaged) [19-21]. The scientific literature also shows results in that sol-gel coatings can be applied to medical implants in order to protect them from corrosion in the body and/or to improve the tissue's biological response [22]. The synthesis by the sol-gel method of hybrid systems composed of silicates is a new route in the preparation of materials for bioactive implants with improved mechanical properties. Future implants must adapt to regeneration of bone tissue rather than bone replacement. Composite materials containing silicates should promote osteogenic performance of osteoblast cells [23]. There are reports available in the literature on the synthesis of $Bi_{12}SiO_{20}$ thin films using the sol–gel method [2, 24-26] but, there are not studies of the biocompatibility properties of BSO films on AISI316L substrates.

In the present study, system BSO was synthesized via sol-gel method at room temperature. These stable soles were formed in molar concentrations 0.75, 0.90 and 1.05 using as precursors tetraethyl orthosilicate Si $(OC_2H_5)_4$ and Bismuth nitrate (III) pentahydrate $Bi(NO_3)_3{\cdot}5H_2O$, acetic acid $C_2H_4O_2$ and 2-Ethoxyethanol $C_4H_{10}O_2$ as solvents, and as complexing Ethanolamine C_2H_7NO. A commercial AISI 316L austenitic stainless steel (SS) with a composition of Fe-16.42 Cr-11.24 Ni-2.12 Mo-0.020 C-0.37 Si-1.42 Mn-0.011 S-0.040 P (in *wt*.%) is used in this work as substrate. The films were deposited by spin coating at 1500 rpm. Additionally, the films were characterized topographically by Atomic Force Microscopy AFM, Scanning Electron Microscopy SEM, X-ray diffraction XRD, the thickness was measured and biocompatibility test were developed. It was found that the growth of cells is homogeneous on the surface of the coatings indicating that the medium offered by the films does not present active cytotoxicity and surpass in a large number the cellular growth level compared to stainless steel. This study allowed establishing the potential offered by coatings in applications of biocompatibility.

2. Experiment

The chemicals used in this study were ttetraethyl orthosilicate Si$(OC_2H_5)_4$ (Aldrich, 98%) and bismuth nitrate (III) pentahydrate $Bi(NO_3)_3{\cdot}5H_2O$ (Alfa Aeser, 98%) as the precursors, 2-ethoxyethanol (Aldrich, 99%) and glacial acetic acid (Aldrich, 99.7+%) as the solvents and ethanolamine (Aldrich, 98%) as the complex agent.

2.1. Preparation of BSO composite

For the deposition of the BSO films, the sol was prepared by modifying the method proposed by Veber *et al.* [4]. Sols synthesis was established in the following sequence: Solution A containing the 98% pure $Bi(NO_3)_3{\cdot}5H_2O$ (10 g) was dissolved in the acetic acid (25 ml) under constant stirring for 2 h at room temperature. Solution B contained tetraethyl orthosilicate (0.38 ml) diluted with 2-ethoxyethanol to the molar concentration M1=0.75, M2=0.90 and M3=1.05, under constant stirring for 1/2 h at room temperature. Subsequently, the solutions A and B were mixed under constant stirring for 1 h. Finally, the ethanolamine was added to adjust the pH=4 and to protect the bismuth ions from hydrolysis. Due to the large amount of water in $Bi(NO_3)_3{\cdot}5H_2O$, was vacuum dried by 96 h at 70 °C. Figure 1 shows the scheme followed in the synthesis.

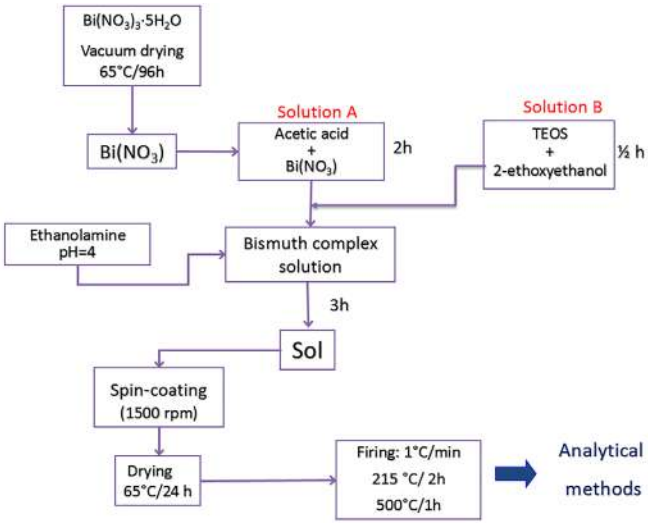

Figure 1 BSO synthesis sol

2.2. BSO thin films

Once a sol was obtained, the films were deposited by spin-coating on samples of 316 L stainless steel of size 3.5 cm x 2.5 cm x 0.32 cm. Before deposition, the substrates were polished to metallographic brightness and were cleaned off unwanted residue (oil, dust, and residual metals) with acetone in ultrasonic bath for 10 minutes. Then dried using hot air for 3 minutes before the deposition of coating. All the films were carried out at room temperature by spin-coating with speed of 1500 rpm and rotation time of 10 seconds.

The films in the different molar concentrations were conformed with a time of aging of 500 h of sol, approximately. They were dried in oven for 24 h at 65 °C. The sintering of the films was carried out at a speed of heating of 1 °C/min, so: the temperature rises from 65 °C to 215 °C staying constant for two hours, soon it is taken to 500 °C and it is stabilized by one hour and finally, it was cooled until getting room temperature at the speed of cooling of the furnace, Figure 1.

2.3. Characterization

The data on morphology and element composition of the surface were obtained using a SUPERPROBE JXA-8100 microprobe X-ray spectral analyzer (JEOL, Japan) and S-5500 scanning electron microscope (Hitachi, Japan) with the system for energy-dispersive X-ray spectral microanalysis. In the case of microprobe analysis, the element composition of the coating surface was determined on 5 randomly selected areas of a size of 300 x 200 μm2, and the obtained data were averaged. The analysis depth was up to 5 μm.

Surface topographical modifications of thin films were investigated by NaioAFM - Nanosurf. The AFM images were taken in the contact mode in ambient. The area selected for the measurement was 46,2 x 46,2 μm. The number of points was 256 and the time per point was 1 second and the measurement was repeated 2 times per zone.

To determine the crystalline structure, a Panalitycal-Emperean diffractometer was used with the copper Kα line (1.540998 Å). Measurements were made with a current intensity of 30 mA, a potential difference of 40 kV, and with a 20° to 90° (2θ) sweep configured with a step time of 0.50 s and a step size of 0.020° (2θ) in continuous mode, in the measurements of XRD the geometric configuration Bragg-Brentano was used.

To measure the thickness, a DEKTAK 150 profilometer with 6 Å repeatability was used. The measurements were made with a sweep of 600 μm, with duration of 30 s, applying a force of 1 mg, with profile of valleys and ridges, and resolution of 0.067 μm / sample.

Biocompatibility assays include:

Cell adhesion: For this assay cells were seeded on films surface and substrate-316L surface. Incubated for 24 hours in 500 μl of culture medium under conditions Standard, as described above. After incubation, cells without adhering were removed by four washes with sterile water. Cells that remained attached surface to the substrate and films were fixed and stained with 300 μl of a solution composed of 0.1% toluidine blue and 3.5% paraformaldehyde. After 24 hours at room temperature, 100 μl of the supernatant was used to measure the optical absorption at 630 nm by an enzyme-linked immunosorbent assay [27].

Cellular proliferation: This assay is based on the ability of the mitochondrial succinate dehydrogenase enzyme for the metabolic reduction of 3-(4,5-dimethylthiazol-2-yl)-2,5-diphenyltetrazole (MTT), this reduction results in a blue colored compound (formazan) which determines the mitochondrial functionality of the treated cells. This assay has been used to measure cell proliferation; wherein the number of live cells is proportional to the amount of formazan produced [27].

Cells were seeded and incubated for 24, 48, 120, 144 and 168 hours; Fresh medium and antibody (500 μl) were added daily to the cultures. At the end of each term, the cells were incubated with 60 μl of MTT at 37 ° C for 4 hours. The supernatant was then removed and 250 μl of dimethyl sulfoxide (DMSO) was added to each well. After 30 minutes of incubation, the absorbance at 570 nm was measured [27].

3. Results and discussion

3.1. SEM

Figure 2 exhibits the topography of the BSO coating. The dark areas correspond to the coating while the bright areas correspond to the growth of bismuth oxide-silicon. Micrographs were taken with a magnification of 1000x.

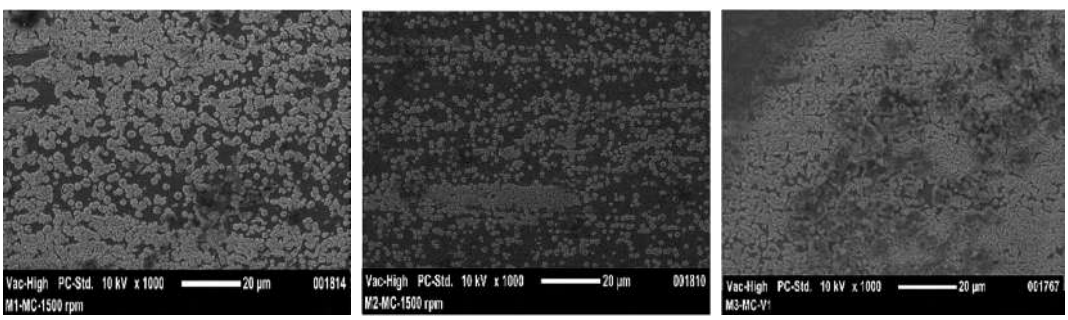

Figure 2 SEM images of coatings as a function of molar concentration. a) M1=0.75, b) M2=0.90 and c) M3=1.05

Figure 3 allows detailed observation of the surface coating M1 and corresponding chemical elemental microanalysis. The presence of oxides of silicon and bismuth are evidenced. Information elements such as iron, chromium and nickel elements corresponding to the substrate composition are also identified, Figure 3 and Table 1.

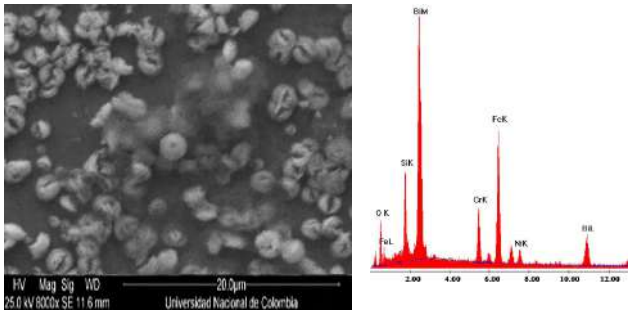

Figure 3 Detail of the coating in molar concentration M1=0.75. a) SEM image and b) Chemical elemental analysis

Table 1 Chemical elemental analysis

Element	Wt %.
OK	10.62
SiK	6.63
CrK	6.71
FeK	21.52
NiK	3.07
BiL	51.45

Figure 4 illustrates in detail three regions of the coating failure M2: substrate zone, film zone and granular zone. In the elementary chemical analysis (Figure 4(b) and Table 2), coating delamination was related to the deep dark area while in the granular area the growth of oxide particles with greatest contribution element Bi was observed (Figure 4(c) and Table 3). The appearance of Bi-Si oxides is due to sintering process applied in the consolidation of the coatings on the 316L SS substrate.

Table 2 Substrate chemical elemental analysis

Element	Wt %.
SiK	1.02
SK	0.93
CrK	17.69
FeK	69.8
NiL	10.49

Table 3 Granular chemical elemental analysis

Element	Wt %.
CK	20.11
OK	6.54
SiK	9.07
CrK	1.58
FeK	5.3
NiK	1.08
BiM	56.31

3.2. AFM

Figure 5 shows the topography of the coatings of BTO system. The coatings, regardless of the molar concentration used, M1, M2 or M3, are irregular, showing high values of roughness (Table 4) compared to the sample without coating.

Table 4 Roughness values

Sample	Roughness (nm)
M1	318.5 ± 0.2
M2	187.4 ± 0.6
M3	302.8 ± 0.5
316L SS	45.5 ± 0.2

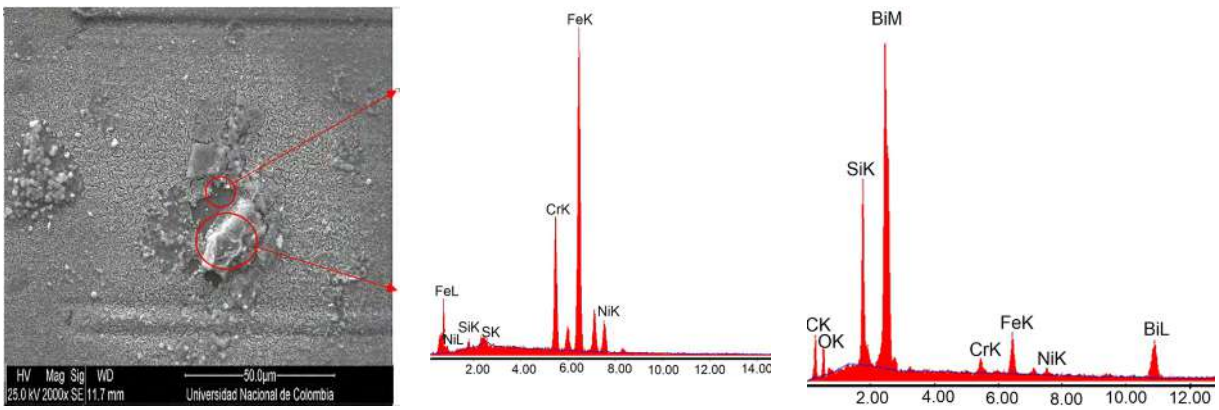

Figure 4 Detail of the coating in molar concentration M2=0.90. a) SEM image, b) Substrate chemical elemental analysis and c) Granular chemical elemental analysis

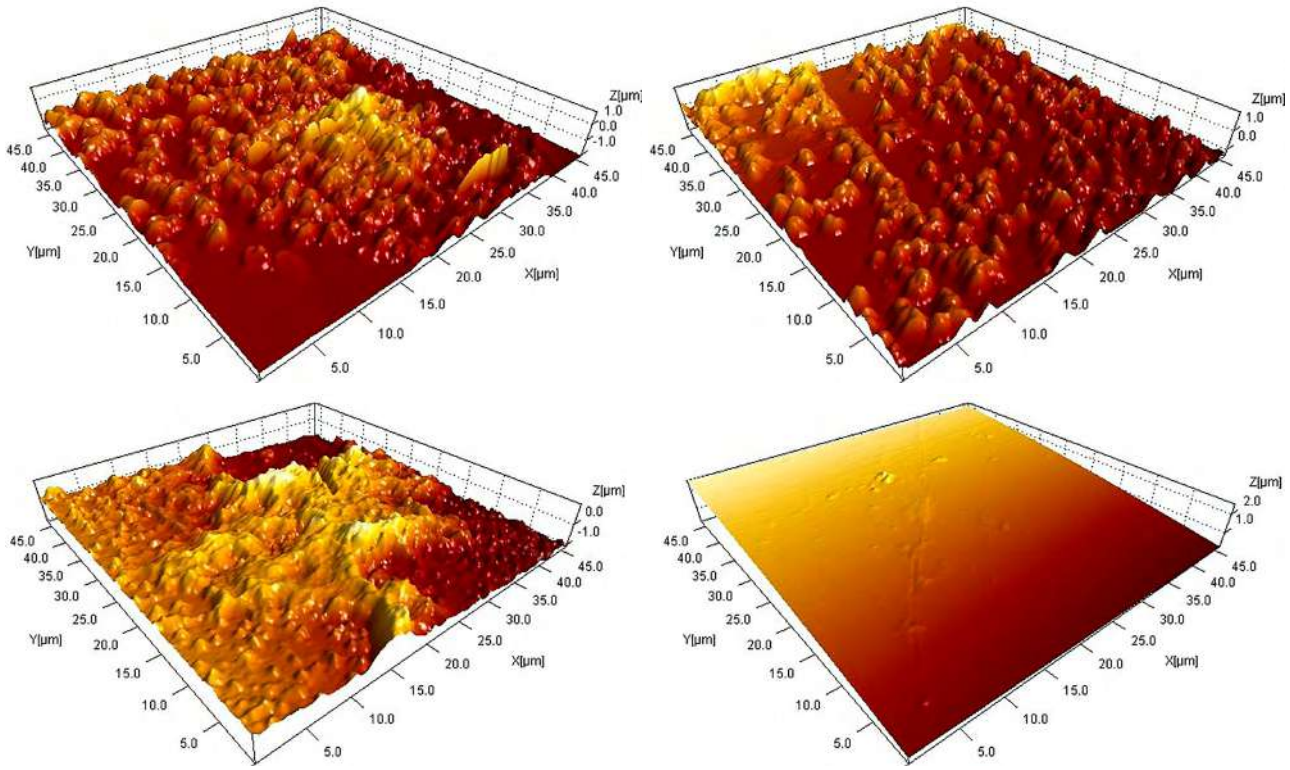

Figure 5 AFM images of coatings as a function of molar concentration. a) M1=0.75, b) M2=0.90 c) M3=1.05 and d) 316L substrate

Table 4 lists the roughness values for the coatings and the substrate. The results allow determining that the coatings obtained from the M1 concentration are more irregular, the films obtained from the concentration M2 are more regular and therefore its roughness value is the lowest of the three.

Figure 5 allows establishing the size of the grains that are on the surface of each coatings. As mentioned in the SEM section, these granules are formations of bismuth oxides and silicon oxides. From Figure 5(a), it is established that the grain sizes for coatings of the molar concentration M1 range from 0.25 µm to 1.50 µm. For the coatings M2 (Figure 5(b)) a grain size between 0.1 µm and 1.8 µm is established. Finally, the Figure 5(c)) shows particle sizes for M3 films, ranging from 0.1 µm to 2 µm.

It is necessary to study the surface morphology of coatings because it is an important feature to consider in cell proliferation, just as surface chemistry is relevant in the protein interactions of cells. It is also necessary to consider the hydroxyl and carboxyl groups present in the coatings which are responsible for the hydrophilic character allowing the incorporation of water molecules and the formation of a network which retains the proteins necessary for cellular nutrition [28, 29].

The wetting ability is also influenced by the surface characteristics of the substrates and / or coatings. Research has been carried out on the so-called "lotus effect" [30-33], where it is concluded that roughness minimizes the area of contact between the surface edges and the cell membrane, inducing a hydrophobic effect of an original hydrophilic surface [29].

As discussed above, in addition to surface chemistry, topography of coatings is an important factor in improving cell or tissue response and its influence on cellular interactions, such as osteoblast adhesion and biomineralization.

3.3. DRX

The diffractograms show the structure sillenite ($Bi_{12}O_{20}Si$) found in all coatings, according to standard chart PDF 98-002-5849. Diffraction patterns exhibit the same behavior. This is explained, because the conditions at which the films were sintered were kept constant, i.e. equal heating rate, temperature and residence time in the furnace. This means that from the structural point of view there is no difference between the films obtained as a function of the variation of tetraethyl orthosilicate concentration. Also, the behavior of the patterns is because the difference between the concentrations of the films studied does not show a significant change in the sillenite structure.

The positions of the main characteristic peaks of the sillenite were found for angles 2θ: 24.696°, 49.099°, 50.828°, 58.9306°, 74.8346 ° and 76.2042 °; with interplanar distances corresponding to 3.602 Å, 1.854 Å, 1.5659 Å, 1.2677 Å and 1.2483 Å, respectively. Figure 6 indicates the positions of the characteristic peaks of the $Bi_{12}O_{20}Si$ found in coatings of the BSO system.

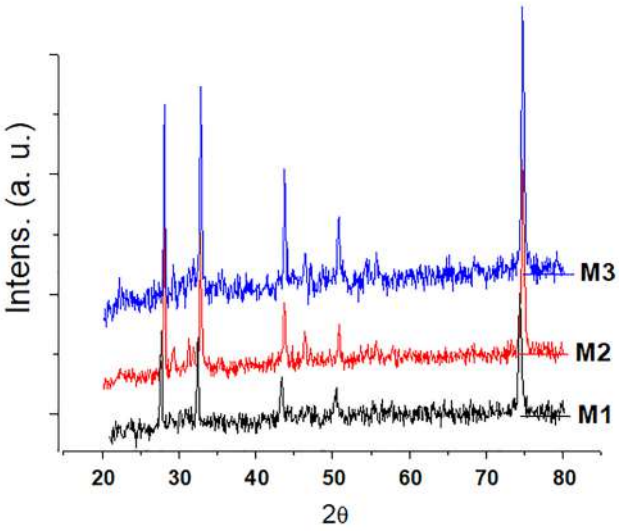

Figure 6 Diffraction pattern of the coatings of the BSO system as a function of the concentration of the precursors (M1, M2 and M3 concentration)

3.4. Film thickness

The results of the measurement of the thicknesses for the films M1, M2 and M3 as a function of the molar concentration are recorded in Table 5. The effect of the addition of Tetraethyl orthosilicate on the final thickness of the coating is evident. Thus, films with less precursor in their composition result in thicker surfaces because the granular growth of bismuth oxides and silicon oxides is favored, as corroborated by SEM and AFM images.

Table 5 Film thickness values

Sample	Film thickness (nm)
M1	390.88 ± 0.25
M2	264.58 ± 0.45
M3	293.97 ± 0.72

3.5. Cell adhesion test

Figure 7 shows the cell adhesion results of the osteoblast species with a 24-hour incubation time. The absorbance levels of the osteoblasts exhibit a growth and adhesion directly proportional to the molar concentration of the films (TEOS), specifically the coatings M3. In Figure 8 it is shown that the degree of cell adhesion of the osteoblasts is directly proportional to the incubation period. This behavior implies that the final composition of the coatings is involved in cell growth processes. It can be inferred that all coatings studied establish optimum cell growth conditions compared to uncoated AISI 316L steel substrates. The graph indicates that the M3 concentration coating presents the best levels of cellular absorbance, which increases cell reproduction.

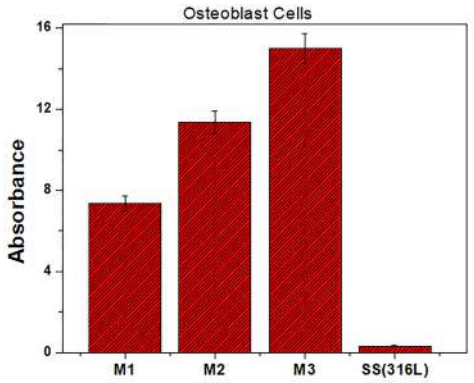

Figure 7 Adhesion of osteoblast cells to 24 h incubation

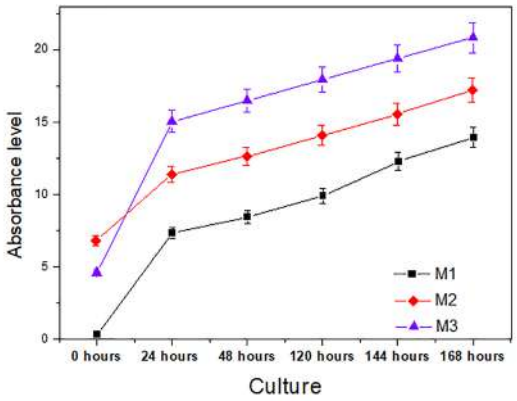

Figure 8 Cell proliferation of osteoblasts for 24, 48, 120, 144 and 168 hours

3.6. Cytotoxicity and cell proliferation with MTT assay

The cell proliferation results for osteoblast cells during an incubation period of 168 hours, incubated on the coatings of the BSO system, are presented in Figure 8. It is concluded that the growth of osteoblasts is homogeneous in the surface of the coatings indicating that the medium offered by the films does not present active cytotoxicity and exceed in large number the level of cellular growth compared to stainless steel [27].

Regarding the cytotoxicity curves in each of the coatings; It is observed that the coating with higher cellular level is M3. The above behavior is explained by the binding of the cells and the surface of the material by Van der Waals forces and by the surface tension generated between the surface of the material and the integrin biomolecules that generate hydrogen bridges. In this way, a protein binding is generated which is adsorbed on the surface of the coating. Integrins on the surface of the material contribute to the tissue organization by binding to extracellular matrix and basement membrane molecules on the surface of the material. The cell factor gives the bio-molecular junction a monatomic layer with the surface oxides and the more complex molecular layers [34, 35].

4. Conclusions

According to the results of this study, and from its discussion and analysis, the following three main conclusions can be drawn: 1) Films were possible to consolidate BSO system at different concentrations of TEOS on 316L SS substrates by spin coating technique. 2) AFM and SEM techniques have been used to investigate the surface morphological features of BSO thin films under the various molar concentrations of TEOS. 3) The topographic characterization, through the SEM and AFM techniques, of the coatings shows very rough films due to the surface growth of bismuth and silicon oxides. 4) It was evidenced the direct influence of the concentration of bismuth nitrate on the roughness of the coatings, and 5) All the coatings presented a crystalline formation evidencing a sillenite structure $Bi_{12}O_{20}Si$. 6) The absorbance levels of the osteoblasts exhibit a growth and adhesion directly proportional to the molar concentration of the films (TEOS), specifically the coatings M3. The cell proliferation results for osteoblast cells during an incubation period of 168 hours, incubated on the coatings of the BSO system, it is concluded that the growth of osteoblasts is homogeneous in the surface of the coatings indicating that the medium offered by the films does not present active cytotoxicity and exceed in large number the level of cellular growth compared to stainless steel.

5. Acknowledgement

The authors wish to thank Dra. Erika Ruiz for technical assistance regarding the assay biocompatibility.

6. References

1. S. Chenab, P. Conflant, M. Drache, J. Boivin, and G. McDonal, "Solid-state reaction pathways of sillenite-phase formation studied by high-temperature X-ray diffractometry and differential thermal analysis," *Materials Research Bulletin*, vol. 38, no. 5, pp. 875–897, 2003.
2. A. Veber, S. Kunej, R. Korosec, and D. Suvorov, "The effects of solvents on the formation of sol–gel-derived Bi12SiO20 thin films," *Journal of the European Ceramic Society*, vol. 30, no. 12, pp. 2475–2480, 2010.
3. S. Fu and H. Ozoe, "Reaction pathways in the synthesis of photorefractive gamma-Bi12MO20 (M = Si, Ge, or Ti)," *J. Am. Ceram. Soc.*, vol. 80, no. 10, pp. 2501–2509, 1997.
4. A. Veber, S. Kunej, and D. Suvorov, "Synthesis and microstructural characterization of Bi12SiO20 (BSO) thin films produced by the sol-gel process," *Ceramics International*, vol. 36, no. 1, pp. 245-250, 2010.
5. E. O. Klebanskii *et al.*, "Thin sol–gel bismuth silicate films," *Phys. Solid State*, vol. 41, no. 6, pp. 913–915, 1999.
6. Y. F. Zhou *et al.*, "Space growth studies of Ce-doped $Bi_{12}SiO_{20}$ single cristal," *Materials Science and Engineering: B*, vol. 113, no. 3, pp. 179–183, 2004.
7. J. Bautista, W. Aperador, A. Delgado, and M. Díaz, "Synthesis and Characterization of Anticorrosive Coatings of SiO2 -TiO2 – ZrO2 Obtained from Sol-Gel Suspensions," *Int. J. Electrochem. Sci.*, vol. 9, no. 8, pp. 4144 - 4157, 2014.
8. C. Brinker and G. Scherer, *Sol–Gel Science: The Physics and Chemistry of Sol–Gel Processing*, 1st ed. San Diego, USA: Academic Press, 1990.
9. A. Amiri, "Solid-phase microextraction-based sol–gel technique," *TrAC Trends in Analytical Chemistry*, vol. 75, pp. 57–74, 2016.
10. M. Oubaha, A. Gorin, C. McDonagh, B. Duffy, and R. Copperwhite, "Development of a multianalyte optical sol–gel biosensor for medical diagnostic," *Sensors and Actuators B: Chemical*, vol. 221, pp. 96–103, 2015.
11. X. Wu *et al.*, "Mechanically robust superhydrophobic and superoleophobic coatings derived by sol–gel method," *Materials & Design*, vol. 89, pp. 1302–1309, 2016.
12. K. Rubesova, V. Jakes, T. Hlasek, P. Vasek, and P. Matejka, "Gel stabilization in chelate sol–gel preparation of Bi-2223 superconductors," *Journal of Physics and Chemistry of Solids*, vol. 73, no. 3, pp. 448–453, 2012.
13. W. Wang, Q. Chen, Q. Cui, J. Ma, and H. Zhang, "Preparation of c-axis oriented YBa2Cu3O7 polycrystalline ceramics by sol–gel method," *Physica C: Superconductivity and its Applications*, vol. 511, pp. 1–3, 2015.
14. X. G. Cao, S. P. Jiang, and Y. Y. Li "Synthesis and characterization of calcium and iron co-doped lanthanum silicate oxyapatites by sol–gel process for solid oxide fuel cells," *Journal of Power Sources*, vol. 293, pp. 806–814, 2015.
15. D. Setsoafiaa, P. Hing, S. Jung, A. Azad, and C. Lim, "Sol–gel synthesis and characterization of Zn2+ and Mg2+ doped La10Si6O27 electrolytes for solid oxide fuel cells," *Solid State Sciences*, vol. 48, pp. 163–170, 2015.
16. X. Wang *et al.*, "Graphene/titanium carbide composites prepared by sol–gel infiltration and spark plasma sintering," *Ceramics International*, vol. 42, no. 1, pp. 122–131, 2016.
17. Z. Abbasi, M. Bahrololoum, R. Bagheri, and M. Shariat, "Characterization of the bioactive and mechanical behavior of dental ceramic/sol–gel derived bioactive glass mixtures," *Journal of the Mechanical Behavior of Biomedical Materials*, vol. 54, pp. 115–122, 2016.
18. J. Mackenzie and D. Ulrich, *Ultrastructure Processing of Advanced Ceramics*, 2nd ed. New York, USA: Wiley, 1988.
19. L. Fedrizzi, F. Rodriguez, S. Rossi, F. Deflorian, and R. Maggio, "The use of electrochemical techniques to study the corrosion behaviour of organic coatings on steel pretreated with sol–gel zirconia films," *Electrochimica Acta*, vol. 46, no. 24-25, pp. 3715–3724, 2001.
20. A. Nazeri, P. Trzaskoma, and D. Bauer, "Synthesis and Properties of Cerium and Titanium Oxide Thin Coatings for Corrosion Protection of 304 Stainless Steel,"

Journal of Sol-Gel Science and Technology, vol. 10, no. 3, pp. 317-331, 1997.
21. T. Sugama, "Cerium acetate-modified aminopropylsilane triol: A precursor of corrosion-preventing coating for aluminum-finned condensers," *Journal of Coatings Technology and Research*, vol. 2, no. 8, pp. 649-659, 2005
22. S. Areva *et al.*, "Sol-gel-derived TiO2-SiO2 implant coatings for direct tissue attachment. Part II: Evaluation of cell response," *J. Mater. Sci. Mater. Med*. vol. 18, no. 8, pp. 1633–1642, 2007.
23. D. Arcos and M. Vallet, "Sol–gel silica-based biomaterials and bone tissue regeneration," *Acta Biomaterialia*, vol. 6, no. 8, pp. 2874-2888, 2010.
24. S. Plyaka, G.Sokolyanskii, E. Klebanskii, and L. Sadovskaya, "Conductivity of the Bi12SiO20 Thin films," *Condens. Matter Phys*., vol. 2, no. 4, pp. 625–630, 1999.
25. X. Zhu *et al.*, "Synthesis of BSO ($Bi_4Si_3O_{12}$) scintillation thin film by sol–gel method," *Journal of Alloys and Compounds*, vol. 582, pp. 33–36, 2014.
26. H. Weidong, Q. Wei, W. Xiaohong, and N. Hailong, "Thin bismuth oxide films prepared through the sol–gel method," *Materials Letters*, vol. 61, no. 19-20, pp. 4100–4102, 2007.
27. J. Storkert, A. Blásquez, M. Cañete, R. Horobin, and A. Villanueva, "MTT assay for cell viability: Intracellular localization of the formazan product is in lipid droplets," *Acta Histochemica*, vol. 114, no. 8, pp. 785-796, 2012.
28. E. Vogler., "Structure and reactivity of water at biomaterial surfaces," *Adv. Colloid. Interf. Sci*., vol. 74, no. 1-3, pp. 69-117, 1998
29. A. Ochsenbein *et al.*, "Osteoblast responses to different oxide coatings produced by the sol–gel process on titanium substrates," *Acta Biomaterialia*, vol. 4, no. 5, pp. 1506-1517, 2008.
30. C. Neinhuis and W. Barthlott, "Characterization and distribution of water-repellent, self-cleaning plant surfaces," *Annals of Botany*, vol. 79, no. 6, pp. 667-677, 1997.
31. Z. Guo, F. Zhou, J. Hao, and W. Liu, "Stable biomimetic super-hydrophobic engineering materials," *J. Am. Chem. Soc.*, vol. 127, no. 45, pp. 15670-15671, 2005.
32. R. Narhe and D. Beysens, "Water condensation on a super-hydrophobic spike Surface," *Europhys Lett.*, vol. 75, no. 1, pp. 98–104, 2006.
33. N. Blanchemain *et al.*, "Improvement of biological response of YAG Laser irradiated polyethylene," *J. Mater. Chem.*, vol. 17, no. 38, pp. 4041-4049, 2007.
34. A. Lupu and T. Popescu, "The noncellular reduction of MTT tetrazolium salt by TiO_2 nanoparticles and its implications for cytotoxicity assays," *Toxicology in Vitro*, vol. 27, no.5, pp. 1445-1450, 2013.
35. Y. Liu, D. Peterson, H. Kimura, and D. Schubert, "Mechanism of cellular 3-(4,5-dimethylthiazol-2-yl)-2,5-diphenyltetrazolium bromide (MTT) reduction," *J. Neurochem*, vol. 69, no.2, pp. 581-593, 1997.